

Point mass Cosmological Black Holes

Javad T. Firouzjaee and Touhid Fegghi

*School of Astronomy, Institute for Research in Fundamental Sciences (IPM), P. O. Box 19395-5531, Tehran, Iran**

Abstract: Real black holes in the universe are located in the expanding accelerating background which are called the cosmological black holes. Hence, it is necessary to model these black holes in the cosmological background where the dark energy is the dominant energy. In this paper, we argue that most of the dynamical cosmological black holes can be modeled by point mass cosmological black holes. Considering the de Sitter background for the accelerating universe, we present the point mass cosmological background in the cosmological de Sitter space time. Our work also includes the point mass black holes which have charge and angular momentum. We study the mass, horizons, redshift structure and geodesics properties for these black holes.

Contents

I. Introduction	1
II. From dynamical black holes to the point mass black holes	2
III. Point mass CBH	4
IV. Charged Black hole	5
V. Kerr- de Sitter Black hole	7
VI. Cosmological black holes properties	9
A. Misner-Sharp mass	10
B. Redshift	10
C. Black hole boundary	11
D. Circular orbits for CBHs	12
VII. Conclusion	13
References	16

I. INTRODUCTION

After Hubble discovery of the cosmic expansion, people needed to make black hole models which are embedded in the expanding Friedmann-Lemaître-Robertson Walker background. The 1933 McVittie solution [1] was the first attempt to model the point mass black hole in the cosmological background. The McVittie black hole is embedded in a general FLRW background, so that the region between the black hole horizon and cosmological horizon is evolving. Even though this model was used for different black hole modelings, this metric has some basic problems [2] [3] [4]. In this way, some metrics [5] which are introduced cannot present comprehensive properties of the horizon, singularity or matter type.

The main criticism for these metrics is that they manufacture the geometry and attribute it to the black hole models. With this action, matter in the right hand side of the Einstein equation will be restricted, and the black hole horizon and singularity change their position and properties generally. The standard way to derive a metric is to know its matter field and its symmetry. Along this way Lemaître-Tolman-Bondi (LTB) model was introduced which describe the perfect fluid collapse in the spherically symmetric space time [6]. Apart from its dynamical nature, the FLRW is a special case of

*Electronic address: j.taghizadeh.f@ipm.ir, tohid.faghihi@gmail.com

this metric and can be modeled as a background. Since the geometry is not static, the need for a local definition of black holes and their boundaries (horizons) have led to concepts such as an isolated horizon [8], Ashtekar and Krishnans dynamical horizon [9], and Booth and Fairhursts slowly evolving horizon [10]. Inspired by these LTB metric properties, the cosmological black hole (CBH) can be built [11–13] that its singularity and horizon is formed during collapse.

In many respects a CBH shows different properties relative to the stationary black holes. The first evident difference is that in the CBH at least two horizons appear in the model: first the apparent horizon and second the cosmological horizon [15, 16], and the causal structure of the black hole will be different from stationary one. Second, the mass definition of the black hole will need to be extended to the quasi-local masses [14] rather than like a ADM mass. Even though the Hawking radiation from the stationary black hole is revised for CBH case [17]. Now, the question arise as to whether a CBH can be useful relative to the Schwarzschild (stationary metrics) one. The first CBH application is in the primordial black hole modeling [18]. These black holes form when the FLRW background density perturbations exceed some threshold values in the radiation dominated era. Moreover, McVittie CBH is used to model the cosmological defect in the inflationary phase [20]. The second CBH application is to model the structure in the matter dominated era [19] where these models were used to investigate the dark energy, virialization, rotation curve and weak-lensing, etc.

In this paper, in section II we infer the point mass CBH form a big class of CBH which can be used for cosmological structure. Section III, IV and V is devoted to make a point mass CBH in presence of mass, mass-charge and mass-angular momentum. Then, in Section VI we study these black holes mass, horizon, redshift structures and geodesics properties. The conclusion and discussions are given in Section VII.

II. FROM DYNAMICAL BLACK HOLES TO THE POINT MASS BLACK HOLES

The main feature of a dynamical black hole is its matter flux. It was shown [12, 14] that the black hole apparent horizon growth is proportional to the matter flux which falls to it. Here we are interested in the case that the black hole evolves slowly due to the matter flux. First we introduce the dynamical case [9] which is a general slowly evolving horizon and then we consider the slowly evolving case. Geometry of the apparent horizon H is expressed by the unit normal to H by $\hat{\tau}^a$; $g_{ab}\hat{\tau}^a\hat{\tau}^b = -1$. The unit space-like vector orthogonal to S and tangent to H is represented by \hat{r}^a . The rescaling freedom in the choice of null normals will be fixed via $l^a = \hat{\tau}^a + \hat{r}^a$ and $n^a = \hat{\tau}^a - \hat{r}^a$. We introduce the area radius R , a function which is constant on each S and satisfies $a_S = 4\pi R^2$. Now, the 3-volume d^3V on H can be decomposed as $d^3V = |\partial R|^{-1} dR d^2V$ where ∂ denotes the gradient on H . Hence, as we will see, our calculations will simplify if we choose $N_R = |\partial R|$.

We define the flux of energy associated with $\xi_{(R)}^a = N_R \ell^a$ across ΔH as:

$$\mathcal{F}_{\text{matter}}^{(R)} := \int_{\Delta H} T_{ab} \hat{\tau}^a \xi_{(R)}^b d^3V = \frac{1}{G} (M(r_2) - M(r_1)). \quad (1)$$

In the spherically symmetric case $M(r)$ is the Misner-Sharp mass [14]. With calculating this quantity on the apparent horizon

$$\frac{dM}{dt}|_{AH} = (M' \frac{dr}{dt} + \dot{M}). \quad (2)$$

Here $\dot{}$ and \prime are partial differentials relative to t and r respectively. Take a collapsing ideal fluid within a compact spherically symmetric spacetime region described by the following metric in the comoving coordinates (t, r, θ, φ) :

$$ds^2 = -e^{2\nu(t,r)} dt^2 + e^{2\psi(t,r)} dr^2 + R(t,r)^2 d\Omega^2. \quad (3)$$

Assuming the energy momentum tensor for the perfect fluid in the form

$$\begin{aligned} T_t^t &= -\rho(t, r), & T_r^r &= p_r(t, r), \\ T_\theta^\theta &= T_\varphi^\varphi = p_\theta(t, r) = w\rho(t, r), \end{aligned} \quad (4)$$

with the weak energy condition

$$\rho \geq 0 \quad \rho + p_r \geq 0 \quad \rho + p_\theta \geq 0, \quad (5)$$

where w describes the equation of state. Einstein equations give,

$$\rho = \frac{2M'}{R^2 R'} \quad , \quad p_r = -\frac{2\dot{M}}{R^2 \dot{R}}, \quad (6)$$

where M , Misner-Sharp mass, is defined by

$$e^{-2\psi}(R')^2 - e^{-2\nu}(\dot{R})^2 = 1 - \frac{2M}{R}. \quad (7)$$

We can define the matter flux into the apparent horizon matter flux relative to fluid 4-velocity

$$D_t M = \frac{1}{e^\nu} \frac{dM}{dt} \Big|_{AH} = \frac{1}{e^\nu} (M' \frac{dr}{dt} + \dot{M}). \quad (8)$$

Using the Einstein equation [13, 16] we get

$$D_t M = 4\pi R_H^2 (-U) \frac{\rho + p}{1 - 8\pi R_H^2 \rho} \quad (9)$$

where $U = \frac{\dot{R}}{e^\nu}$. At first glance, we can see that the matter (flux) on the apparent becomes zero when density becomes zero on the apparent horizon. We define this quantity which characterize the slowly evolving horizon [10] when

$$\epsilon^2 = \alpha \theta_n^2 R_H^2 \ll 1. \quad (10)$$

This quantity in the spherically symmetric space time becomes [13]

$$\epsilon^2 = 4\pi R_H^2 \frac{(1+w)\rho}{1 - 4\pi R_H^2 (1-w)\rho} \quad (11)$$

To have an slowly evolving black hole with mass $M = 2R_H$ the energy density for this black hole, ρ , must be small. In the special case the $\epsilon = \rho = 0$ we get the isolated horizon [8] which the matter flux is zero.

Proposition: If a dynamical black hole evolves and finally its horizon becomes isolated, the space time geometry around the black hole horizon becomes Schwarzschild metric with the same Misner-Sharp mass.

If the horizon becomes isolated i.e. $\epsilon = 0$ then the energy density becomes zero, $\rho = p = 0$. Hence we have underdensity (vacuum) around the black hole horizon. On the other hand we know that the vacuum solutions of the Einstein equation around a spherically symmetric mass distribution have Schwarzschild form

$$ds^2 = -(1 - \frac{2C}{R})dt^2 + (1 - \frac{2C}{R})^{-1}dR^2 + R^2 d\Omega^2. \quad (12)$$

Using the fact the $M = 2R_H$ is the apparent horizon for Schwartzchild metric (as boundary condition), we get $C = M$. Therefore, in the isolated horizon case the space time geometry around horizon becomes Schwarzschild with the same Misner-Sharp mass.

Located in the cosmological background, the CBH collapsing part separates from the expanding part and the density between them decreases. This underdense region is usually called void in the cosmology. As a result, the matter flux can not exist forever and after sometime it decreases [12, 14]. In this case as inferred above taking the black hole as a point mass is a good model.

III. POINT MASS CBH

In the last section we inferred that since the matter and matter flux around the black hole decrease and the black hole mass is bigger than the total matter around it, the point mass black hole can be a good model for CBH. On the other side the cosmological constant is the best model to describe the cosmic acceleration which we called it dark energy in the matter sector. The de Sitter metric is the Einstein equation solution with the cosmological constant. Since the dark energy is the main cosmological matter (about 70 %) and all other matter (dark matter and baryonic matter) located in the matter flux which have fall in the black hole and made a point mass black hole, then it is sufficient to find the point mass black hole in the cosmological de Sitter background. One may think that the Schwarzschild-de Sitter is a good metric for the CBH, but Schwarzschild-de Sitter has been written in the static coordinate. Consequently it is needed find the Schwarzschild-de Sitter metric in the cosmological coordinate to present the point mass CBH.

Since the standard cosmological metrics are written in the synchronous coordinate, we first have to transform the Schwarzschild-de Sitter to the synchronous coordinates. We know that the Schwarzschild-de Sitter metric is given by

$$ds^2 = -\Phi dt^2 + \Phi^{-1} dR^2 + R^2 d\Omega^2, \quad (13)$$

where

$$\Phi = 1 - \frac{\Lambda}{3} R^2 - \frac{2M}{R}. \quad (14)$$

By these coordinate transformations [21]

$$\begin{aligned} d\tau &= dt - \frac{\sqrt{1-\Phi}}{\Phi} dR, \\ dr &= -dt + \frac{1}{\Phi\sqrt{1-\Phi}} dR, \end{aligned} \quad (15)$$

metric (13) will be

$$ds^2 = -d\tau^2 + \left(\frac{2M}{R} + \frac{\Lambda}{3} R^2\right) dr^2 + R^2 d\Omega^2. \quad (16)$$

To find R as a function of r and τ we can use

$$\int d\tau + dr = \int \frac{dR}{\sqrt{1-\Phi}}. \quad (17)$$

Therefore, we can write

$$\tau + r = \int \frac{dR}{\sqrt{\frac{\Lambda}{3} R^2 + \frac{2M}{R}}} = \frac{2}{\sqrt{3}\Lambda} \ln(\Lambda R^{\frac{3}{2}} + \sqrt{6M\Lambda + \Lambda^2 R^3}). \quad (18)$$

Hence, we can write R

$$R = \frac{e^{-\sqrt{\frac{\Lambda}{3}}(r+\tau)} (e^{\sqrt{3\Lambda}(r+\tau)} - 6\Lambda M)^{\frac{2}{3}}}{2^{\frac{2}{3}} \Lambda^{\frac{2}{3}}}. \quad (19)$$

As a result, we can write the Schwarzschild-de Sitter metric in the cosmological form

$$\begin{aligned} ds^2 &= -d\tau^2 + \left[\frac{2M}{\left(\frac{e^{-\sqrt{\frac{\Lambda}{3}}(r+\tau)} (e^{\sqrt{3\Lambda}(r+\tau)} - 6\Lambda M)^{\frac{2}{3}}}{2^{\frac{2}{3}} \Lambda^{\frac{2}{3}}} \right)} + \frac{\Lambda}{3} \left(\frac{e^{-2\sqrt{\frac{\Lambda}{3}}(r+\tau)} (e^{\sqrt{3\Lambda}(r+\tau)} - 6\Lambda M)^{\frac{4}{3}}}{2^{\frac{4}{3}} \Lambda^{\frac{4}{3}}} \right) \right] dr^2 \\ &\quad + \left(\frac{e^{-2\sqrt{\frac{\Lambda}{3}}(r+\tau)} (e^{\sqrt{3\Lambda}(r+\tau)} - 6\Lambda M)^{\frac{4}{3}}}{2^{\frac{4}{3}} \Lambda^{\frac{4}{3}}} \right) d\Omega^2. \end{aligned} \quad (20)$$

In the limit where the black hole mass tend to zero, the metric $\lim_{M \rightarrow 0} ds^2$ will be

$$\begin{aligned} ds^2 &= -d\tau^2 + \frac{\Lambda}{3} \frac{(e^{2\sqrt{\frac{\Lambda}{3}}}(r+\tau))}{(2\Lambda)^{\frac{4}{3}}} dr^2 + \frac{(e^{2\sqrt{\frac{\Lambda}{3}}}(r+\tau))}{(2\Lambda)^{\frac{4}{3}}} d\Omega^2 \\ &= -d\tau^2 + \frac{e^{2\sqrt{\frac{\Lambda}{3}}}\tau}{(2\Lambda)^{\frac{4}{3}}} \left[\frac{\Lambda}{3} e^{2\sqrt{\frac{\Lambda}{3}}r} dr^2 + e^{2\sqrt{\frac{\Lambda}{3}}r} d\Omega^2 \right]. \end{aligned} \quad (21)$$

By redefining $S = \frac{e^{2\sqrt{\frac{\Lambda}{3}}r}}{(2\Lambda)^{2/3}}$ we get

$$ds^2 = -d\tau^2 + e^{2\sqrt{\frac{\Lambda}{3}}\tau} [dS^2 + S^2 d\Omega^2], \quad (22)$$

which is de Sitter metric.

With calculating the Ricci scalar, we can see that the singularity is located at $r + \tau = \frac{1}{\sqrt{3\Lambda}} \ln(6\Lambda M)$ that is equivalently $r = 0$.

The Penrose-Carter diagram of these black holes can be seen in the Fig.(1).

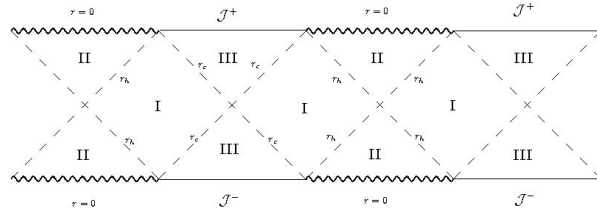


FIG. 1: Penrose-Carter diagram of maximally extended Schwarzschild-de Sitter black hole.

These black holes properties will be discussed in Section VI.

IV. CHARGED BLACK HOLE

If we add charge to a point mass we get the Reissner Nordstrom solution. If we solve the Einstein equation with cosmological constant and a point mass with charge we get the de Sitter-Reissner Nordstrom solution. Here we use Carter's spherically symmetric three parameter (M,Λ,Q) solution to Einstein's equations where Q is the electric charge of black hole [22]. The metric in static coordinates is

$$ds^2 = -\Phi dt^2 + \Phi^{-1} dR^2 + R^2 d\Omega^2, \quad (23)$$

where

$$\Phi = 1 - \frac{\Lambda}{3} R^2 - \frac{2M}{R} + \frac{Q^2}{R^2}. \quad (24)$$

By coordinate transformations given by (15), the metric (23) will be

$$ds^2 = -d\tau^2 + \left(\frac{\Lambda}{3} R^2 + \frac{2M}{R} - \frac{Q^2}{R^2} \right) dr^2 + R^2 d\Omega^2. \quad (25)$$

We can write

$$\tau + r = \int \frac{dR}{\sqrt{\frac{\Lambda}{3} R^2 + \frac{2M}{R} - \frac{Q^2}{R^2}}}. \quad (26)$$

If we define $G(R) = \int \frac{dR}{\sqrt{\frac{\Lambda}{3}R^2 + \frac{2M}{R} - \frac{Q^2}{R^2}}}$ then $R = G^{-1}(\tau + r)$. We can calculate the inverse function numerically, as if we draw the function $r + \tau = G(R)$ and change the variables $(R, G(R))$ to $(G(R), R)$ and then use numerical methods to find the equation of drawn line.

Because of existence of three free parameters Λ , Q and M this integral requires tedious calculations (if an analytical solution required) to solve, and even after fining the integral it would be much harder to find the inverse function, R , which will give the solution. Hence, we need to suppose some simplifying assumptions. Therefore, at large ' R ' where $\frac{\Lambda}{3}R^2 \gg \frac{2M}{R}, \frac{Q}{R^2}$ or equivalently $R \gg \text{Max}(\sqrt[3]{\frac{6M}{\Lambda}}, \sqrt[4]{\frac{3Q^2}{\Lambda}})$

$$\begin{aligned} \tau + r &= \int \frac{dR}{\sqrt{\frac{\Lambda}{3}R^2 + \frac{2M}{R} - \frac{Q^2}{R^2}}} = \sqrt{\frac{3}{\Lambda}} \int \frac{R^{-1}dR}{\sqrt{1 + \frac{6M}{\Lambda R^3} - \frac{3Q^2}{\Lambda R^4}}} \simeq \sqrt{\frac{3}{\Lambda}} \int R^{-1} [1 - \frac{3M}{\Lambda R^3} + \frac{3Q^2}{2\Lambda R^4}] dR \\ &= \sqrt{\frac{3}{\Lambda}} (\ln(R) + \frac{M}{\Lambda R^3} - \frac{3Q^2}{8\Lambda R^4}). \end{aligned} \quad (27)$$

As a result

$$R = \exp^{\text{RootOf}[8(r+\tau) - \sqrt{\frac{3}{\Lambda}} (\frac{8\Lambda x e^{4x} + 8M e^x - 3Q^2}{\Lambda e^{4x}})]}. \quad (28)$$

For $\lim_{Q, M \rightarrow 0} ds^2$, according to (28), $R = \exp^{\sqrt{\frac{\Lambda}{3}}(r+\tau)}$ and the line element (25) will be (21) and it represents de Sitter metric.

It might be interesting considering the case $M = 0$ ($Q \neq 0$)

$$\int \frac{dR}{\sqrt{\frac{\Lambda}{3}R^2 - \frac{Q^2}{R^2}}} = \frac{1}{2\sqrt{\frac{\Lambda}{3}}} \ln(\Lambda R^2 + \sqrt{\Lambda^2 R^4 - 3\Lambda Q^2}). \quad (29)$$

Then

$$R = \frac{e^{-\sqrt{\frac{\Lambda}{3}}(r+\tau)} \sqrt{e^{4\sqrt{\frac{\Lambda}{3}}(r+\tau)} + 3\Lambda Q^2}}{\sqrt{2\Lambda}} \quad (30)$$

The metric in this case will be

$$\begin{aligned} ds^2 &= -d\tau^2 + \left(\frac{\Lambda}{3} \frac{e^{-2\sqrt{\frac{\Lambda}{3}}(r+\tau)} (e^{4\sqrt{\frac{\Lambda}{3}}(r+\tau)} + 3\Lambda Q^2)}{2\Lambda} - \frac{Q^2}{\frac{e^{-2\sqrt{\frac{\Lambda}{3}}(r+\tau)} (e^{4\sqrt{\frac{\Lambda}{3}}(r+\tau)} + 3\Lambda Q^2)}{2\Lambda}} \right) dr^2 \\ &\quad + \left(\frac{e^{-2\sqrt{\frac{\Lambda}{3}}(r+\tau)} (e^{4\sqrt{\frac{\Lambda}{3}}(r+\tau)} + 3\Lambda Q^2)}{2\Lambda} \right) d\Omega^2. \end{aligned} \quad (31)$$

The singularities are located at $R = 0$ and $R = \sqrt{\frac{3Q^2}{\Lambda}}$.

For $R \ll M$ and $Q \ll M$ equation (26) we will be

$$\begin{aligned} r + \tau &= \int \frac{dR}{\sqrt{\frac{\Lambda}{3}R^2 + \frac{2M}{R} - \frac{Q^2}{R^2}}} = \int \frac{\sqrt{R}dR}{\sqrt{\frac{\Lambda}{3}R^3 + 2M - \frac{Q^2}{R}}} = \int \frac{\sqrt{R}}{\sqrt{2M}} [1 - \frac{Q^2}{2MR} + \frac{\Lambda}{6M} R^3]^{-\frac{1}{2}} dR \\ &\simeq \frac{1}{\sqrt{2M}} \left(\frac{2}{3} R^{\frac{3}{2}} + \frac{Q^2}{2M} R^{\frac{1}{2}} - \frac{\Lambda}{54M} R^{\frac{9}{2}} \right) \end{aligned} \quad (32)$$

and ' R ' will be

$$R = \text{RootOf}[-5832M(r+\tau)^2 + 729M^2Q^2x + 1944MQ^2x^2 + 1296x^3 - 54\Lambda M^2Q^2x^5 - 72\Lambda Mx^6 + \Lambda^2M^2x^9]. \quad (33)$$

The Penrose-Carter diagram of these black holes can be seen in the Fig.(2).

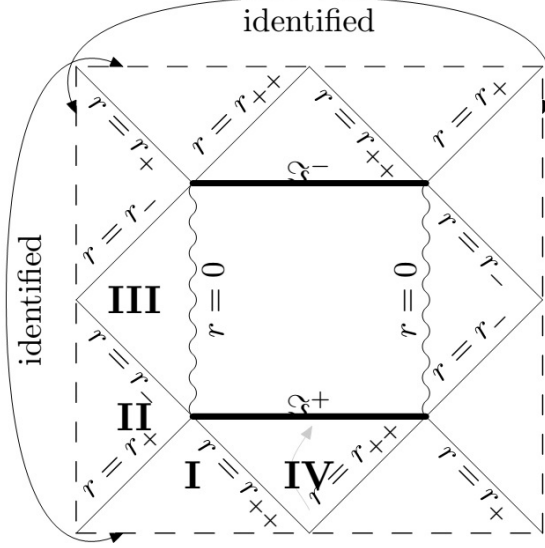


FIG. 2: Penrose-Carter diagram of the maximally extended de Sitter-Reissner Nordstrom solution [23].

V. KERR- DE SITTER BLACK HOLE

In this section we want to describe the point mass CBH with the angular momentum. In Boyer-Lindquist like coordinates employed by Carter, the Kerr-de Sitter line element will be [22] :

$$ds^2 = (R^2 + a^2 \cos^2 \Theta) \left[\frac{dR^2}{\Delta_R} + \frac{d\Theta^2}{1 + \frac{\Lambda}{3} a^2 \cos^2 \Theta} \right] + \sin^2 \Theta \frac{(R^2 + a^2 \cos^2 \Theta)}{1 + \frac{\Lambda}{3} a^2 \cos^2 \Theta} \left[\frac{adt - (R^2 + a^2)d\varphi}{1 + \frac{\Lambda}{3} a^2} \right]^2 - \frac{\Delta_R}{(R^2 + a^2 \cos^2 \Theta)} \left[\frac{dt - a \sin^2 \Theta d\varphi}{1 + \frac{\Lambda}{3} a^2} \right], \quad (34)$$

where

$$\Delta_R = (R^2 + a^2) \left(1 - \frac{\Lambda}{3} R^2 - 2MR \right). \quad (35)$$

The Kerr-de sitter metric is rather complicated , so finding a coordinate in which metric becomes in the form of $ds^2 = \Phi dt^2 - \Phi^{-1} dR^2 - R^2 d\Omega^2$ is elusive. In this way, to simplify metric, we first take $\Theta = 0$ polar cut of the metric and due to axisymmetry φ can be set to equal any value from 0 to 2π . With these assumptions the metric (34) will be

$$ds^2 = \frac{R^2 + a^2}{\Delta_R} dR^2 - \frac{\Delta_R}{R^2 + a^2} \left[\frac{dt}{1 + \Lambda 3a^2} \right]^2. \quad (36)$$

If we suppose $dt' = \frac{dt}{1 + \Lambda 3a^2}$ we will have

$$ds^2 = \frac{R^2 + a^2}{\Delta_R} dR^2 - \frac{\Delta_R}{R^2 + a^2} dt'^2. \quad (37)$$

Similar to the last section if we use coordinate transformations (15) the line element (37) will be

$$ds^2 = -d\tau^2 + \left(\frac{\Lambda}{3} R^2 + \frac{2MR}{R^2 + a^2} \right) dr^2, \quad (38)$$

Where

$$\int d\tau + dr = \int \frac{dR}{\sqrt{1-\Phi}}, \quad (39)$$

And

$$\Phi = \frac{\Delta_R}{R^2 + a^2}. \quad (40)$$

We can write

$$\tau + r = \int \frac{dR}{\sqrt{1 - \frac{\Delta_R}{R^2 + a^2}}} = \int \frac{dR}{\sqrt{\frac{\Lambda}{3}R^2 + \frac{2MR}{R^2 + a^2}}}. \quad (41)$$

Since this integral calculation is complex, we will consider two simple cases $R \ll a$ and $R \gg a$.

For $R \ll a$ we will have

$$\tau + r = \int \frac{dR}{\sqrt{\frac{\Lambda}{3}R^2 + \frac{2MR}{R^2 + a^2}}} \simeq \int \frac{dR}{\sqrt{\frac{\Lambda}{3}R^2 + \frac{2MR}{a^2}}} = \int \frac{dR}{\sqrt{(\sqrt{\frac{\Lambda}{3}}R + \frac{M}{a^2}\sqrt{\frac{3}{\Lambda}})^2 - (\frac{M}{a^2}\sqrt{\frac{3}{\Lambda}})^2}}. \quad (42)$$

Hence we get

$$\tau + r = \frac{1}{\sqrt{\frac{\Lambda}{3}}} \ln \left(\sqrt{\frac{\Lambda}{3}}R + \frac{M}{a^2}\sqrt{\frac{3}{\Lambda}} + \sqrt{-(\frac{M}{a^2}\sqrt{\frac{3}{\Lambda}})^2 + (\sqrt{\frac{\Lambda}{3}}R + \frac{M}{a^2}\sqrt{\frac{3}{\Lambda}})^2} \right). \quad (43)$$

To find 'R' we must find the inverse form of above function, so it will be

$$R = \frac{1}{2\sqrt{\frac{\Lambda}{3}}} \left(\exp\left(\sqrt{\frac{\Lambda}{3}}(r + \tau)\right) - 2\frac{M}{a^2}\sqrt{\frac{3}{\Lambda}} + \left(\frac{M}{a^2}\sqrt{\frac{3}{\Lambda}}\right)^2 \exp\left(-\sqrt{\frac{\Lambda}{3}}(r + \tau)\right) \right). \quad (44)$$

For $R \gg a, M$ we will have

$$\begin{aligned} \tau + r &= \int \frac{dR}{\sqrt{\frac{\Lambda}{3}R^2 + \frac{2MR}{R^2 + a^2}}} \simeq \int \frac{(1 + \frac{a^2}{2R^2})dR}{\sqrt{\frac{\Lambda}{3}R^2 + \frac{2M}{R}}} = \int \frac{dR}{\sqrt{\frac{\Lambda}{3}R^2 + \frac{2M}{R}}} + \int \frac{(\frac{a^2}{2R^2})dR}{\sqrt{\frac{\Lambda}{3}R^2 + \frac{2M}{R}}} \\ &= \sqrt{\frac{3}{\Lambda}} \left[\ln(R) + \frac{M}{\Lambda R^3} \right] + \frac{a^2}{2} \sqrt{\frac{3}{\Lambda}} \left[-\frac{1}{2R^2} + \frac{3M}{5\Lambda R^5} \right]. \end{aligned} \quad (45)$$

Therefore,

$$\tau + r = \sqrt{\frac{3}{\Lambda}} \left[\ln(R) + \frac{M}{\Lambda R^3} \right] + \frac{a^2}{2} \sqrt{\frac{3}{\Lambda}} \left[-\frac{1}{2R^2} + \frac{3M}{5\Lambda R^5} \right]. \quad (46)$$

Since $R \gg a, M$, if we neglect $\frac{1}{R^5}$ term, then we will have

$$R = e^{\text{RootOf}[-4\sqrt{3}\Lambda^{\frac{3}{2}}(r+\tau)e^{3x} + 12\Lambda x e^{3x} - 3\Lambda a^2 e^x + 12M]}. \quad (47)$$

If we only suppose $R \gg a$ (not $R \gg M$) we will have

$$\begin{aligned} \tau + r &= \int \frac{dR}{\sqrt{\frac{\Lambda}{3}R^2 + \frac{2M}{R}}} \simeq \int \frac{(1 + \frac{a^2}{2R^2})dR}{\sqrt{\frac{\Lambda}{3}R^2 + \frac{2M}{R}}} = \int \frac{dR}{\sqrt{\frac{\Lambda}{3}R^2 + \frac{2M}{R}}} + \int \frac{(\frac{a^2}{2R^2})dR}{\sqrt{\frac{\Lambda}{3}R^2 + \frac{2M}{R}}} \\ &= \sqrt{\frac{4}{3\Lambda}} \text{arcsinh}\left(\sqrt{\frac{3\Lambda}{8M}} \frac{2}{3} R^{\frac{3}{2}}\right) + \int \frac{(\frac{a^2}{2R^2})dR}{\sqrt{\frac{\Lambda}{3}R^2 + \frac{2M}{R}}}. \end{aligned} \quad (48)$$

To calculate the integral $\int \frac{(\frac{a^2}{2R^2})dR}{\sqrt{\frac{\Lambda}{3}R^2 + \frac{2M}{R}}}$ we have

$$\int \frac{(\frac{a^2}{2R^2})dR}{\sqrt{\frac{\Lambda}{3}R^2 + \frac{2M}{R}}} = \int \frac{(\frac{a^2}{2R^2})\sqrt{R}dR}{\sqrt{\frac{\Lambda}{3}R^3 + 2M}} = \int \frac{(\frac{a^2}{2})(\frac{3}{2}u)^{(\frac{2}{3})^{-2}}du}{\sqrt{\frac{3\Lambda}{4}u^2 + 2M}}, \quad (49)$$

where we have used $\sqrt{R}dR = du$ or $\frac{2}{3}R^{\frac{3}{2}} = u$. If we use $u^2 = t$, the above integral will be

$$\int \frac{\frac{1}{4a^2}(\frac{3}{2})^{-\frac{2}{3}}t^{-\frac{7}{6}}dt}{\sqrt{\frac{3\Lambda}{4}t + 2M}} = \frac{1}{4a^2}(\frac{3}{2})^{-\frac{2}{3}} \frac{-3(\frac{-\Lambda t}{M})^{\frac{5}{6}}(8M + 3\Lambda t) + 2 * 3^{\frac{1}{6}}\Lambda t \sqrt{8 + \frac{3\Lambda t}{M}} \text{Beta}[-\frac{3\Lambda t}{M}, \frac{5}{6}, \frac{1}{2}]}{2Mt^{\frac{1}{6}}(\frac{-\Lambda t}{M})^{\frac{5}{6}}\sqrt{(8M + 3\Lambda t)}}. \quad (50)$$

According to $t = u^2$ and $u = \frac{2}{3}R^{\frac{3}{2}}$ so $t = \frac{4}{9}R^3$

$$\begin{aligned} \int \frac{(\frac{a^2}{2R^2})dR}{\sqrt{\frac{\Lambda}{3}R^2 + \frac{2M}{R}}} = \\ \frac{1}{4a^2}(\frac{3}{2})^{-\frac{2}{3}} \frac{-3(\frac{-\Lambda(\frac{4}{9}R^3)}{M})^{\frac{5}{6}}(8M + 3\Lambda(\frac{4}{9}R^3)) + 2 * 3^{\frac{1}{6}}\Lambda(\frac{4}{9}R^3)\sqrt{8 + \frac{3\Lambda(\frac{4}{9}R^3)}{M}} \text{Beta}[-\frac{3\Lambda\frac{4}{9}R^3}{M}, \frac{5}{6}, \frac{1}{2}]}{2M(\frac{4}{9}R^3)^{\frac{1}{6}}(\frac{-\Lambda(\frac{4}{9}R^3)}{M})^{\frac{5}{6}}\sqrt{(8M + 3\Lambda(\frac{4}{9}R^3))}}. \end{aligned} \quad (51)$$

Hence if we define

$$\begin{aligned} G(R) = \sqrt{\frac{4}{3\Lambda}} \text{arcsinh}(\sqrt{\frac{3\Lambda}{8M}} \frac{2}{3}R^{\frac{3}{2}}) + \\ \frac{1}{4a^2}(\frac{3}{2})^{-\frac{2}{3}} \frac{-3(\frac{-\Lambda(\frac{4}{9}R^3)}{M})^{\frac{5}{6}}(8M + 3\Lambda(\frac{4}{9}R^3)) + 2 * 3^{\frac{1}{6}}\Lambda(\frac{4}{9}R^3)\sqrt{8 + \frac{3\Lambda(\frac{4}{9}R^3)}{M}} \text{Beta}[-\frac{3\Lambda\frac{4}{9}R^3}{M}, \frac{5}{6}, \frac{1}{2}]}{2M(\frac{4}{9}R^3)^{\frac{1}{6}}(\frac{-\Lambda(\frac{4}{9}R^3)}{M})^{\frac{5}{6}}\sqrt{(8M + 3\Lambda(\frac{4}{9}R^3))}}, \end{aligned} \quad (52)$$

Then we get

$$R = G^{-1}(r + \tau). \quad (53)$$

Therefore, we present point mass CBH with angular momentum with finding the G function.

The Penrose-Carter diagram of these black holes can be seen in the Fig.(3).

VI. COSMOLOGICAL BLACK HOLES PROPERTIES

From the last sections discussion a question arises as to whether we can see the trace of the cosmological constant (which play the cosmological acceleration role) in the observation. To make an estimate consider the Schwarzschild-de Sitter metric in the stationary coordinate (14). Since the R value is invariant due to the transformation to the cosmological coordinate, we can compare the two terms $\frac{\Lambda}{3}R^2$ from cosmological constant and $\frac{2m}{R}$ from the black hole. In cosmology the value $\frac{\Lambda}{3} = H_0^2$ where the $H_0 = 67.74 \pm 0.46 \text{ km/s/Mpc} = 2.195 \pm 0.01510^{-18} \text{ s}^{-1}$ is the Hubble constant at the present time. For a black hole with the sun mass m_\odot at scale $R \gtrsim 10^{18}m = 100pc$ the cosmological constant term cannot be negligible. In this scale some phenomena of black hole like lensing [25] and Cosmic Microwave Background distortion from primordial black hole are important and we have to use the cosmological constant model to describe them. In this part we investigate what happen for black hole mass, boundary and redshift structure if someone take the cosmological coordinate.

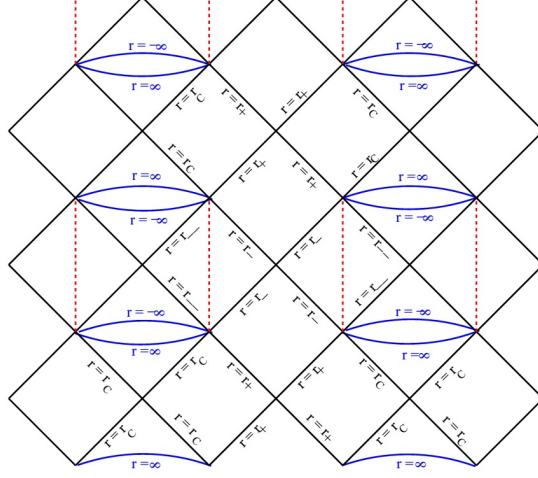


FIG. 3: Penrose-Carter diagram of the maximally extended Kerr-de Sitter solution [24].

A. Misner-Sharp mass

The spherically symmetric metric can be written

$$ds^2 = \gamma_{ab} dx^a dx^b + R^2 d\Omega^2. \quad (54)$$

where $a, b : (t, r)$. In this form the Misner-Sharp mass which is defined for the spherically symmetric space time [14] becomes

$$M_{ms} = \frac{R}{2} (1 - \gamma^{ab} \partial_a R \partial_b R) \quad (55)$$

Since $\gamma^{ab} \partial_a R \partial_b R$ is invariant under the coordinate transformation $(t, r) \rightarrow (t', r')$ the Misner-Sharp mass is also invariant under these transformation.

Since the coordinate transformation from the stationary Schwarzschild-de Sitter coordinate to the cosmological coordinate has only the (t, r) part, as a result, spherically symmetric cosmological black holes the Misner-Sharp will be the same Schwarzschild charge de Sitter mass:

$$M_{ms} = \frac{R}{2} (1 - \gamma^{ab} \partial_a R \partial_b R) = m + \frac{\Lambda}{6} R^2 - \frac{Q}{2R}. \quad (56)$$

One can also calculate the matter flux for above cosmological black hole in the spherically symmetric case. It can be shown from equation (8) that the matter flux is zero for these CBHs. This verifies that these CBH are point mass CBHs.

B. Redshift

If an emitter sends a light ray to an observer with null vector k^μ , the relative light redshift that is calculated by observer with 4-velocity u^μ is,

$$1 + z = \frac{w_e}{w_o} = \frac{(k_\mu u^\mu)_e}{(k_\mu u^\mu)_o}, \quad (57)$$

where the light null geodesic k^μ is normalized with the affine parameter. It can be shown that the affinnary null geodesics equation

$$k^\nu k_{;\nu}^\mu = 0 \quad (58)$$

will not change from coordinate transformation. As a result, the affine parameter will remain the same. Hence, it results that the redshift properties of a spacetime for an observer will not change due to the coordinate transformation.

Consequently, the infinite redshift surface for the above CBHs will be the same infinite redshift surface in the stationary coordinate.

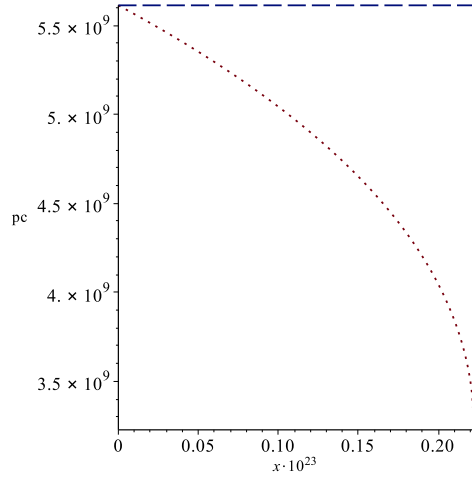


FIG. 4: de Sitter event horizon as a function of mass. Dash line represents de Sitter event horizon for $m = 0$.

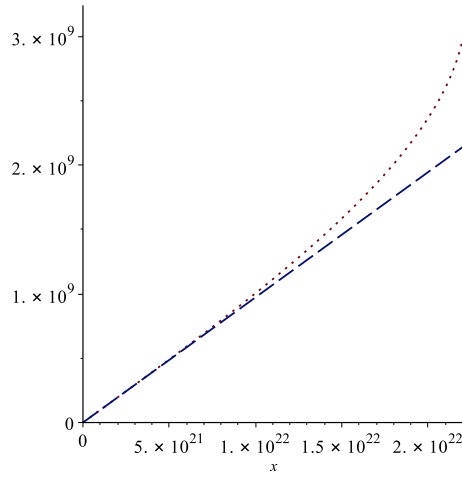


FIG. 5: Black hole event horizon as a function of mass. Dash line represents black hole event horizon for $\Lambda = 0$.

C. Black hole boundary

The event horizon is usually used to define the black hole boundary in textbooks. Since the event horizon definition is a global quantity and we have to know all information about the spacetime evolution finally, we need to define a quasi-local quantity which can be applied for real dynamical black hole in numerical relativity. To solve this problem people use the apparent horizon to define the black hole boundary in a dynamical case [9, 10, 13].

Black hole boundary definition: A smooth, three-dimensional, space-like sub-manifold (possibly with boundary) H of space-time is said to be a trapping horizon if it can be foliated by a family of

closed 2-manifolds such that on each leaf S the expansion $\theta_{(\ell)}$ of one null normal ℓ^μ vanishes; and the expansion $\theta_{(n)} < 0$ of the other null normal n^μ is negative. This surface separates the trapped surface, $\theta_{(n)}, \theta_{(\ell)} < 0$, from untrapped one $\theta_{(n)} < 0$, $\theta_{(\ell)} > 0$.

In the spherically symmetric space time the black hole the black hole boundary is located on the apparent horizon $\theta_{(\ell)} = 0$. In terms of normal metric components it becomes $\gamma^{ab}\partial_a R \partial_b R = 0$.

Since $\gamma^{ab}\partial_a R \partial_b R$ is invariant under the coordinate transformation $(t, r) \rightarrow (t', r')$ the black hole boundary or apparent horizon is invariant under these transformation.

Point mass CBHs have two horizons. The first is cosmological horizon and the second horizon is black hole horizon (event or apparent horizon). For the point mass CBH (20) there is also two black hole and cosmological horizon. Since the coordinate transformation do not change the horizons location, it is sufficient to find roots of Φ in the Schwarzschild-de Sitter spacetime. Note that the infinite redshift surface is the same black hole horizon surface in the stationary coordinate. Hence, the infinite redshift surface will be the same black hole apparent horizon for these CBHs. It can easily be shown that the expansion of outgoing null geodesics is proportional to Φ , which $\Phi = 0$ determines the position of horizons. We can depict the roots of $\Phi = 1 - \frac{\Lambda}{3}R^2 - \frac{2m}{R}$ for $\Lambda = 10^{-52}s^{-1}$ as a function of $x = \frac{m}{m_\odot}$ where m_\odot is the sun mass. There are three real roots for $\Phi = 0$ if $\Lambda m^2 \leq \frac{1}{9}$ [26], where one of them is negative, so we consider $R_C = \frac{2}{\sqrt{\Lambda}} \cos(\frac{\cos^{-1}(-3\sqrt{\Lambda}m)}{3})$ and $R_H = \frac{2}{\sqrt{\Lambda}} \cos(\frac{\cos^{-1}(-3\sqrt{\Lambda}m)}{3} + \frac{4\pi}{3})$ which are cosmological and black hole event horizons respectively.

Two cosmological and black hole horizons are depicted in Fig.(4) Fig.(5). It can be seen that using standard value of dark energy, the astrophysical black hole with mass $m < 10^{10}m_\odot$ can not change the cosmological horizon place. On the other side, the standard value of cosmological constant does not change the black hole horizon place significantly.

D. Circular orbits for CBHs

In cosmology and astrophysics, many events and physics such as microlensing, dark matter, missing satellite, stars velocity dispersion and etc. emerge from the studying of object orbits where most of them are simplified by circular orbits. In this part, we study the possibility of the circular orbits around the CBHs (without charge and angular momentum).

Circular orbits are characterized by a constant radius. In a stationary coordinate like Schwarzschild de Sitter coordinate there is well defined coordinate R which is the areal coordinate, but in the cosmological coordinate we have two comoving and areal radius. Since the angular distance is proportional to the areal radius we choose the areal radius as a circular orbits radius. As a consequence of time and radius coordinate transformation from stationary Schwarzschild-de Sitter to the CBH cosmological coordinate, the areal coordinate will not changes. As a result, the circular coordinate in both frames are the same, but are labeled by different coordinates. Here we want to study the form of effective potential in Schwarzschild-de Sitter spacetime to study the circular orbits. We can use Euler Lagrange Equations with metric (13) which is spherically symmetric and so we can choose $\Theta = \frac{\pi}{2}$. The Euler Lagrange equations will result:

$$\begin{aligned} \epsilon &= -\Phi \dot{t}^2 + \Phi^{-1} \dot{R}^2 + R^2 \dot{\varphi}^2 \\ \dot{t} &= \frac{E}{\Phi} \\ \dot{\varphi} &= \frac{L}{R^2}, \end{aligned} \tag{59}$$

where dot is partial differential relative to affine parameter and E and L are constants. $\epsilon = -1, 0, 1$ represents timelike, null and spacelike geodesics respectively. From the equation (59) we can introduce effective potential $V(R)$, where

$$V(R) = E^2 - \dot{R}^2 = \Phi(R) \left(\frac{L^2}{R^2} - \epsilon \right) \tag{60}$$

We can depict $V(R)$ as a function of $\frac{M}{R}$ for different values of L and α where $\alpha = 9\Lambda M^2$ and $0 \leq \alpha \leq 1$, that $\alpha = 1$ is the extreme case.

If we suppose a massless particle at infinity has the initial velocity $v_0^r = \sqrt{E^2 + V(\infty)}$, as the massless particle moves toward central object, it decelerates to $\sqrt{E^2 - V(r)}$ and if $E^2 > V_{max}$, the zero mass particle will accelerate toward singularity otherwise \dot{r} will change sign and the particle will be reflected to infinity. According to figure (6) and (7) as we decrease Λ or increase L , it becomes harder for these particles to fall in to singularity. We can also study the circular orbits for mass less particles. We know that if $\frac{\partial V}{\partial r} = 0$ and $\dot{R} = 0$, then we will have circular orbits and the stability criterion is $\frac{\partial^2 V}{\partial R^2} > 0$. Hence we can write

$$\begin{aligned} \frac{\partial V}{\partial R} = 0 &\rightarrow R = 3M \\ \dot{R} = 0 &\rightarrow E^2 = V(R). \end{aligned} \quad (61)$$

According to figure (6), $(\frac{\partial^2 V}{\partial R^2})|_{R=3M} < 0$, that means there is no stable circular orbit for mass less particles except when $E = L = 0$ and $R = 3M$. By equation (61), if we define critical impact parameter as $b = \frac{L}{E}$, then we can write:

$$b = \frac{L}{E} = \left(\sqrt{\frac{R^2}{\Phi(R)}} \right)_{R=3M} = \frac{3\sqrt{3}M}{\sqrt{1-\alpha}}. \quad (62)$$

If the impact parameter of these mass less particles is greater than critical value, then these particles will be captured. This definition leads to a relation for capture cross section for massless particles from infinity:

$$\sigma_{null} = \pi b^2 = \frac{27\pi M^2}{1-\alpha}. \quad (63)$$

We can do the same calculations for the timelike circular orbits. In this case we have

$$\frac{\partial V}{\partial R} = 0 \rightarrow L^2 = \frac{MR^2 - \frac{\Lambda}{3}R^5}{R - 3M}. \quad (64)$$

By equation (64) and $\dot{R} = 0$ one can easily show:

$$E^2 = V(R) = \frac{(1 - \frac{\alpha}{27M^2}R^2 - \frac{2M}{R})^2}{R(R - 3M)}. \quad (65)$$

According to equation (65) it's clear that circular orbits exist for $R > 3M$, but figure (8) tells us that effective potential is convex for the given values of cosmological constant, so there is no circular orbit for time like case at these values. The value of α for a black hole with mass 10^6 sun mass and $\Lambda = 10^{-52}s^{-1}$ is in order of 10^{-32} , in this case we can have stable circular orbit and bound orbit (figure (12)). Figure (8) also represents that for a same value of central mass if we increase the cosmological constant, \dot{R} increases. For a same value of Λ , figure (9) shows that any variation of L in the timelike case is similar to null one.

Figure (10) shows that the spacelike case inside the de Sitter horizon resembles the null and timelike cases, but for outside de sitter horizon as we increase Λ (for same vale of central mass), \dot{R} decreases.

Figure (12) and (13) represent effective potential for a specific black hole with mass $10^6 M_\odot$ and $L = 5M$ and $3M$. We have also used present value of $\Lambda = 10^{-52}s^{-1}$. We can see that only for some values of L we can have timelike circular orbits and bound orbits.

VII. CONCLUSION

Real black holes in the universe, called the cosmological black holes, are located in the expanding accelerating background. These black holes are generically dynamical and they are sourced by baryons

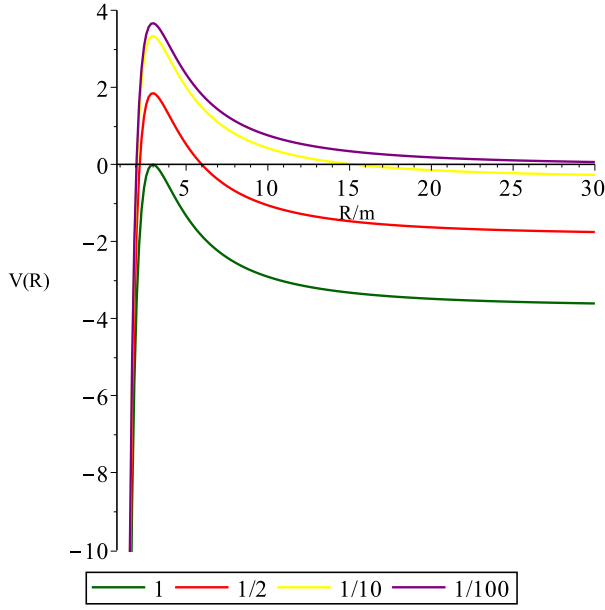


FIG. 6: Effective potential of null geodesics as a function of $\frac{R}{M}$ for different values of α . Here we have supposed $L = 10M$

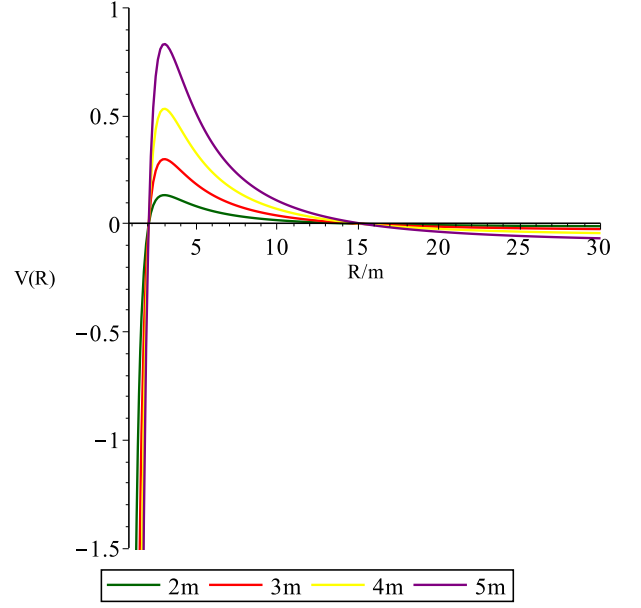


FIG. 7: Effective potential of null geodesics as a function of $\frac{R}{M}$ for different values of L . Here we have supposed $\alpha = \frac{1}{10}$

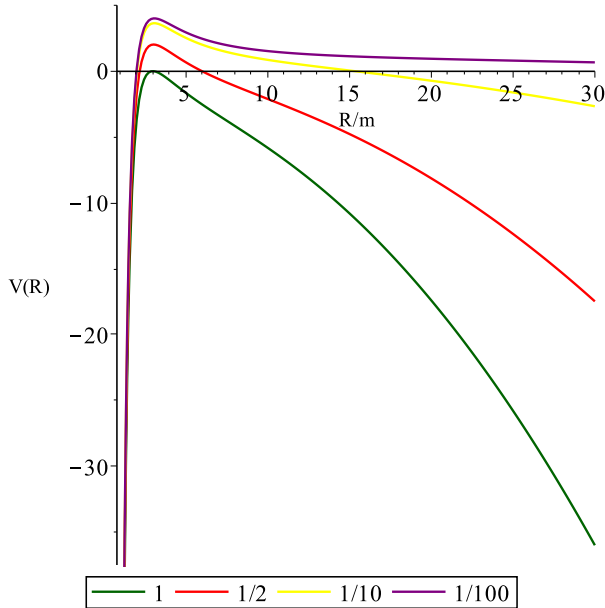


FIG. 8: Effective potential of timelike geodesics as a function of $\frac{R}{M}$ for different values of α . Here we have supposed $L = 10M$.

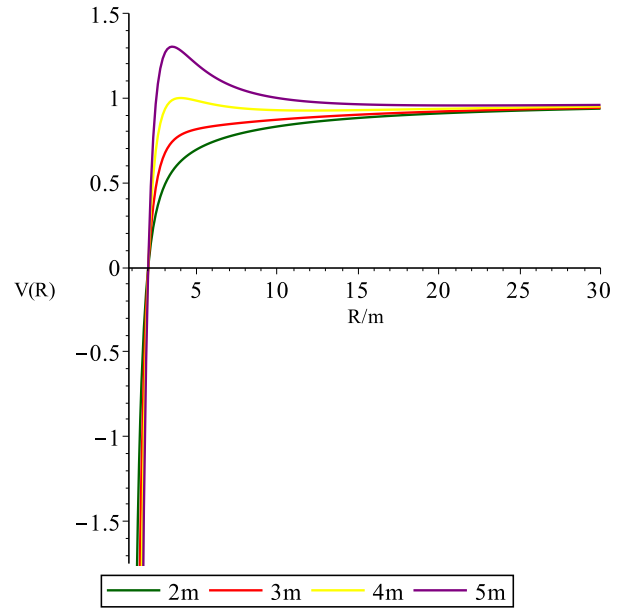


FIG. 9: Effective potential of timelike geodesics as a function of $\frac{R}{M}$ for different values of L . Here we have supposed $\alpha = \frac{1}{10}$.

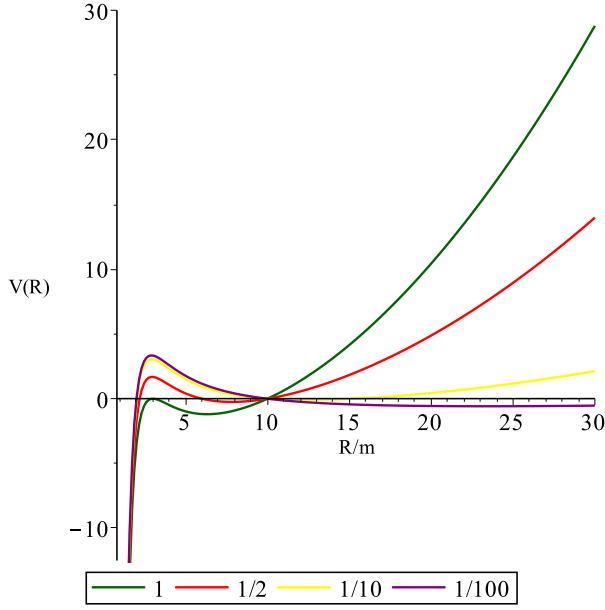


FIG. 10: Effective potential of spacelike geodesics as a function of $\frac{R}{M}$ for different values of α . Here we have supposed $L = 10M$.

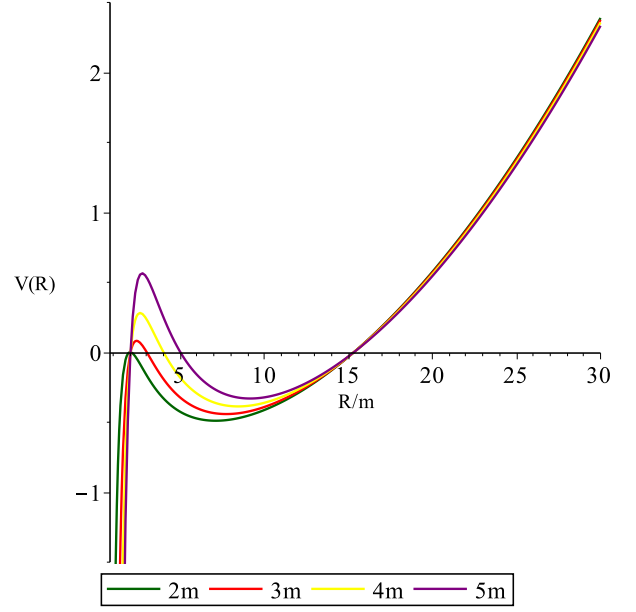


FIG. 11: Effective potential of spacelike geodesics as a function of $\frac{R}{M}$ for different values of L . Here we have supposed $\alpha = \frac{1}{10}$.

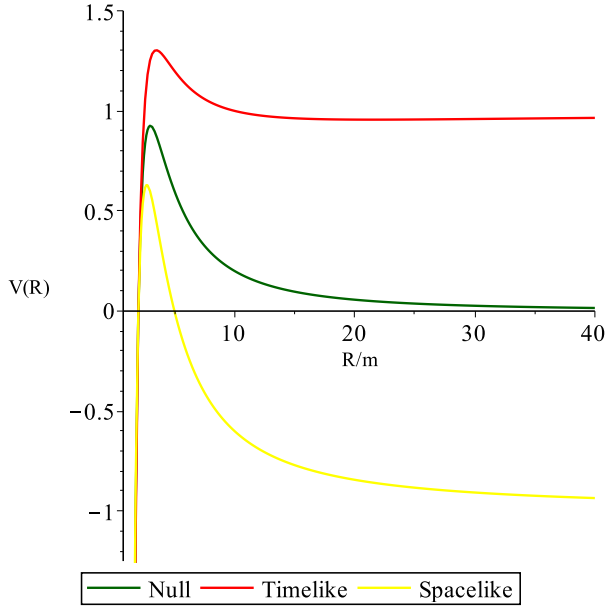


FIG. 12: Effective potential of spacelike, null and timelike geodesics as a function of $\frac{R}{M}$ for a black hole with mass $10^6 M_\odot$ and $\Lambda = 10^{-52} s^{-1}$. Here we have supposed $L = 5M$.

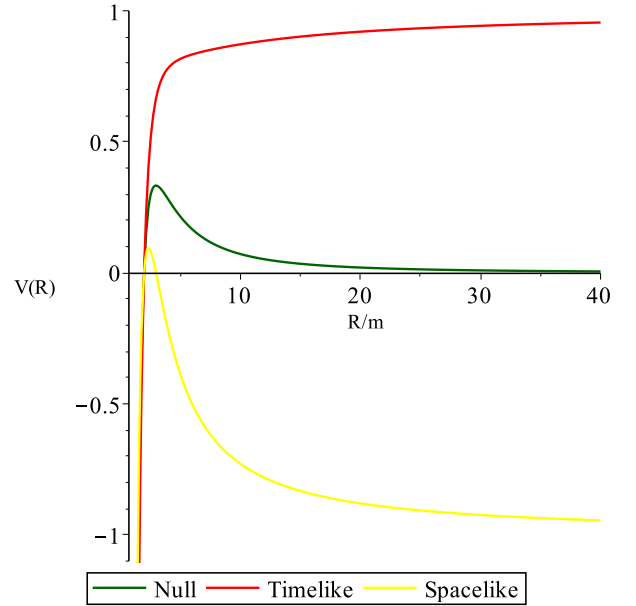


FIG. 13: Effective potential of spacelike, null and timelike geodesics as a function of $\frac{R}{M}$ for a black hole with mass $10^6 M_\odot$ and $\Lambda = 10^{-52} s^{-1}$. Here we have supposed $L = 3M$.

and dark matter. It's been shown that the background expansion leads to voids. These voids are formed between the black hole and the expanding background and prevent the black hole's matter flux from increasing. After this phase of the black hole evolution, the black holes can be approximated as a point mass. In this case the black hole mass is much greater than the matter flux around it. In this paper, we argue that most of the dynamical cosmological black holes can be modeled by point mass cosmological black holes finally. The point mass cosmological background is modeled by the de Sitter space time. We find the Schwarzschild-de Sitter metric in the cosmological coordinate and infer that this metric is the best candidate for the point mass CBH. This metric locally describes a point mass black hole and at large distance reduces to the cosmological de Sitter space time. We also find the point mass black holes solution with charge and angular momentum. We show that the mass, horizons and redshift structure of these black holes will not change due to the coordinate transformation from stationary coordinate to the cosmological coordinate. From studying the effective potential for different geodesics cases it has been shown that the stable circular orbits can exist similar to the stationary case.

Future work [27] will concentrate on studying the astrophysical and cosmological observables of these black holes and compare them with stationary ones.

Acknowledgments:

We would like to thank Alireza Allahyari for useful comments.

-
- [1] G. C. McVittie, Mon. Not. Roy. Astron. Soc. **93**, 325 (1933).
 - [2] B. C. Nolan, Class. Quant. Grav. **16**, 1227 (1999).
 - [3] N. Kaloper, M. Kleban and D. Martin, Phys. Rev. D **81**, 104044 (2010).
 - [4] K. Lake and M. Abdelqader, Phys. Rev. D **84**, 044045 (2011).
 - [5] D. A. Szafron, J. Math. Phys. **18**, 1673 (1977); M. L. McClure and C. C. Dyer, Class. Quant. Grav. **23**, 1971 (2006); V. Faraoni and A. Jacques, Phys. Rev. D **76**, 063510 (2007). I. Antoniou and L. Perivolaropoulos, Phys. Rev. D **93**, no. 12, 123520 (2016).
 - [6] ; R. C. Tolman, Proc. Nat. Acad. Sci. **20**, 169 (1934) [Gen. Rel. Grav. **29**, 935 (1997)]; H. Bondi, Mon. Not. Roy. Astron. Soc. **107**, 410 (1947).
 - [7] A. Krasinski and C. Hellaby, Phys. Rev. D **69**, 043502 (2004); K. Bolejko, M. N. Celerier and A. Krasinski, Class. Quant. Grav. **28**, 164002 (2011); W. Valkenburg, Gen. Rel. Grav. **44**, 2449 (2012); V. Marra and M. Paakkonen, JCAP **1201**, 025 (2012); C. Gao, X. Chen, Y. G. Shen and V. Faraoni, Phys. Rev. D **84**, 104047 (2011); S. Upadhyay, Annals Phys. **356**, 299 (2015); P. Jaluvkova, E. Kopteva and Z. Stuchlik, arXiv:1602.01266 [gr-qc]; M. Korkina and E. Kopteva, Space, Time and Fundamental Interactions. 2012. V. 1, p. 38 - 47.
 - [8] A. Ashtekar, C. Beetle, O. Dreyer, S. Fairhurst, B. Krishnan, J. Lewandowski and J. Wisniewski, Phys. Rev. Lett. **85**, 3564 (2000).
 - [9] A. Ashtekar and B. Krishnan, Phys. Rev. Lett. **89**, 261101 (2002).
 - [10] I. Booth and S. Fairhurst, Phys. Rev. Lett. **92**, 011102 (2004).
 - [11] J. T. Firouzjaee and R. Mansouri, Gen. Rel. Grav. **42**, 2431 (2010).
 - [12] R. Moradi, J. T. Firouzjaee and R. Mansouri, arXiv:1301.1480 [gr-qc]; R. Moradi, Javad T. Firouzjaee and R. Mansouri, Class. Quant. Grav. **32**, no. 21, 215001 (2015).
 - [13] J. T. Firouzjaee, Int. J. Mod. Phys. D **21**, 1250039 (2012).
 - [14] J. T. Firouzjaee, M. P. Mood and R. Mansouri, Gen. Rel. Grav. **44**, 639 (2012).
 - [15] Faraoni, Valerio. "Horizons." Cosmological and Black Hole Apparent Horizons. Springer International Publishing, 2015.
 - [16] A. Helou, I. Musco and J. C. Miller, arXiv:1601.05109 [gr-qc].
 - [17] H. Saida, T. Harada and H. Maeda, Class. Quant. Grav. **24**, 4711 (2007); J. T. Firouzjaee and R. Mansouri, Europhys. Lett. **97**, 29002 (2012); J. T. Firouzjaee and G. F. R. Ellis, Gen. Rel. Grav. **47**, no. 2, 6 (2015); J. T. Firouzjaee and G. F. R. Ellis, arXiv:1511.04316 [gr-qc].
 - [18] B. J. Carr and S. W. Hawking, Mon. Not. Roy. Astron. Soc. **168**, 399 (1974); I. Musco and J. C. Miller, Class. Quant. Grav. **30**, 145009 (2013); T. Harada and S. Jhingan, arXiv:1512.08639 [gr-qc].
 - [19] A. Krasinski and C. Hellaby, Phys. Rev. D **69**, 023502 (2004); M. Razbin, J. T. Firouzjaee and R. Mansouri, Int. J. Mod. Phys. D **23**, no. 09, 1450074 (2014); T. Buchert, Class. Quant. Grav. **28**, 164007 (2011); V. Marra and A. Notari, Class. Quant. Grav. **28**, 164004 (2011); R. Javadinezhad, J. T. Firouzjaee and R. Mansouri, Phys. Rev. D **93**, no. 2, 023007 (2016).

- [20] H. Firouzjahi, A. Karami and T. Rostami, arXiv:1605.08338 [astro-ph.CO]; H. T. Cho, K. W. Ng and I. C. Wang, JCAP **1411**, no. 11, 023 (2014).
- [21] J. Podolsky, Gen. Rel. Grav. **31**, 1703 (1999).
- [22] B. Carter in Les Astres Occlus ed. by DeWitt, C. M. Dewitt, (Gordon and Breach, New York, 1973).
- [23] A. Belhaj, P. Diaz and A. Segui, Phys. Rev. D **80**, 044015 (2009).
- [24] S. Akcay and R. A. Matzner, Class. Quant. Grav. **28**, 085012 (2011).
- [25] M. P. Mood, J. T. Firouzjaee and R. Mansouri, Phys. Rev. D **88**, 083011 (2013); M. P. Mood, J. T. Firouzjaee and R. Mansouri, arXiv:1304.5062 [astro-ph.CO].
- [26] J. Guven, D. Nunez, Phys. Rev. D **42**, 2577, (1990)
- [27] Touhid Feghhi and Javad T. Firouzjaee, in preparation.